Hierarchical analysis of the degradation of fibre-reinforced polymers under the presence of void imperfections

Wilfried V. Liebig, Karl Schulte and Bodo Fiedler

Technische Universität Hamburg-Harburg, Institute of Polymer Composites, Denickestrasse 15, 21073 Hamburg, Germany

WVL, 0000-0003-1855-6237; KS, 0000-0001-6521-0488;
BF, 0000-0002-2734-1353

The subject of this work is the investigation of the influence of voids on the mechanical properties of fibre-reinforced polymers (FRPs) under compression loading. To specify the damage accumulation of FRPs in the presence of voids, the complex three-dimensional structure of the composite including voids was analysed and a reduced mechanical model composite was derived. The hierarchical analysis of the model composite on a micro-scale level implies the description of the stress and strain behaviour of the matrix using the photoelasticity technique and digital image correlation technology. These studies are presented along with an analytical examination of the stability of a single fibre. As a result of the experimental and analytical studies, the stiffness of the matrix and fibre as well as their bonding, the initial fibre orientation and the fibre diameter have the highest impact on the failure initiation. All these facts lead to a premature fibre–matrix debonding with ongoing loss of stability of the fibre and followed by kink-band formation. Additional studies on the meso-scale of transparent glass FRPs including a unique void showed that the experiments carried out on the model composites could be transferred to real composites.

This article is part of the themed issue 'Multiscale modelling of the structural integrity of composite materials'.

1. Introduction

The formation of voids cannot be avoided when manufacturing composite structures. Experimental studies

as well as experience have shown that voids significantly affect the mechanical properties of composite laminates. In particular, the compressive strength of a laminate is reduced even at small void contents. As the mere reduction of the void content beyond a certain level is associated with exponentially increasing costs, the focus today is to get a better understanding about void formation and void impact on failure initiation and propagation, especially.

The compressive strength is in fact a limiting design factor because of its poor performance in comparison with the very high tensile strength. Only ≈60% of the tensile strength could be reached [1]. A further reduction to 50% could be the result of defects like voids [2–4]. In previous works, most efforts were devoted to describing the influence of voids on fibre-reinforced polymer (FRP) properties as a function of void volume content. Particularly with regard to the compressive strength, the void content can have a significant influence as summarized by Schultheisz & Waas [5]. Bazhenov *et al.* [2] investigated both the link between compressive strength and void content as well as the influence of fibre diameter. They concluded that, for thicker fibre diameters, the compressive strength can not only be explained by microbuckling analysis. For modelling the influence, Lee & Soutis [6] suggested to use the fibre microbuckling model by Budiansky [7] to indirectly predict the compressive strength in the presence of voids. Such an approach was first implemented by Gehrig [4] in which the reason for premature failure was disregarded.

To understand why void loaded composites fail or how failure mechanisms interact, it is necessary to reduce the complexity when modelling to a manageable amount, as reported by Liebig *et al.* [8]. This leads to the development of a hierarchical analysis on micro-, meso- and macro-scales to study the degradation of FRPs under the presence of voids as presented in this work.

2. Model composite

Owing to the complex morphology of FRP on the microstructure level, a model composite was developed. It allows one to study the material behaviour in the vicinity of a unique void and to observe the failure mechanisms under external loading. Based on previous investigations with the common prepreg material HexPly M21/35%/134/T800S (M21/T800S) provided by Hexcel Corporation, the void morphology was determined. Therefore, the autoclave pressure was varied during curing between 7, 5, 3 and 1 bar to achieve different void volume contents. The morphology and the position of voids inside the laminate were analysed by using light microscopy, scanning electron microscopy and microcomputer tomography. In real composites, there are three established methods to obtain this information non-destructively: X-ray and ultrasonic technology as well as optical coherent tomography. Within FRP one could distinguish between two different void configurations: intralaminar and interlaminar, as schematically shown in figure 1 [8,9].

Intralaminar voids occur between fibres exhibiting a high length/width ratio, whereas interlaminar voids can be observed in resin-rich areas squeezed between plies, typically showing an irregular shape. Characteristics of the void geometry, i.e. length, width and height, can be defined as its elongation in the fibre direction and dimension in plane and out of plane of the laminate, respectively. However, both void configurations could be consolidated by a representative model composite, as shown in figure 2. The overall cross section is divided into three areas: area I is characterized by parallel fibres with perfect alignment, whereas due to the displacements of the void inclusion the fibres show a slight waviness or misalignment in area II. For both areas many publications can be found describing the influence of fibre orientation on the composite behaviour under compression load [7,10–12]. In this work, we focus on the direct void, area III.

(a) Analytical approach

A minimized number of constituents leads to a model composite, as shown in figure 3. The model consists of a beam (fibre) embedded in the matrix. For both fibre and matrix, i.e. beam and
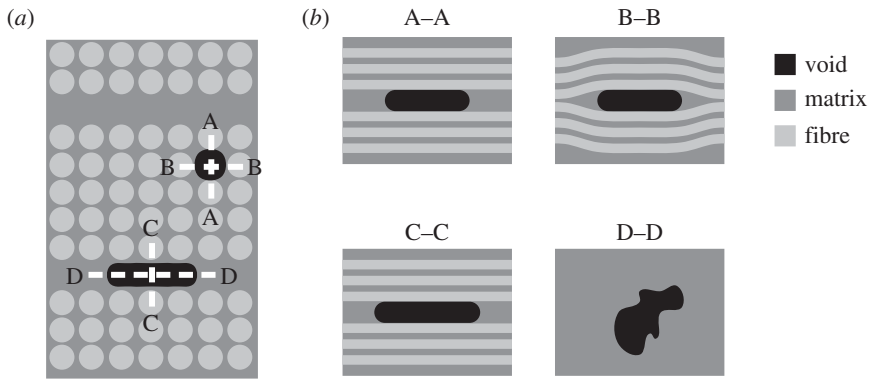
3

rsta.royalsocietypublishing.org *Phil. Trans. R. Soc. A* **374:** 20150279

Figure 1. (*a*) Conformal sketch of intralaminar (sections A and B) and interlaminar (sections C and D) voids and (*b*) the cross sections through void inclusions [8].
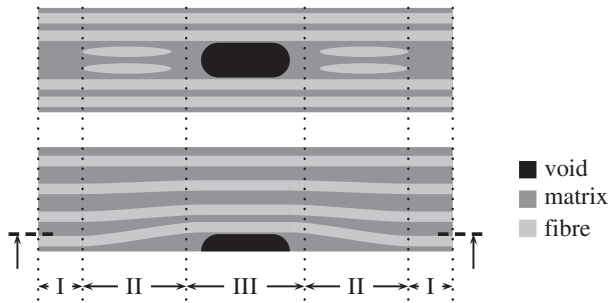

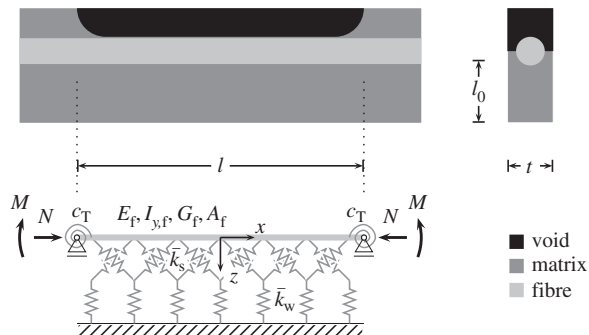**Figure 2.** Schematic of cross section B–B (see also figure 1*b*) [8].

Figure 3. Sketch of the developed model consisting of a Timoshenko beam on a Winkler/Pasternak foundation.

foundation, small deformation and linear elastic and isotropic material behaviour is assumed. Fibre deformation is adopted by Timoshenko's theory [13,14], while the matrix is represented by the elastic foundation of Winkler [15] and Pasternak [16].

The potential energy Π of an axially loaded fibre on Winkler/Pasternak foundation is the sum of the elastic strain energy U and the work of loads W,

$$\Pi = U - W. \tag{2.1}$$

The elastic energy consists of

$$U = \frac{1}{2} \int_{-l/2}^{+l/2} E_f I_{y,f} \left(\frac{\partial \psi(x)}{\partial x} \right)^2 dx + \frac{1}{2} \int_{-l/2}^{+l/2} \kappa G_f A_f \left(\psi(x) + \frac{\partial w(x)}{\partial x} \right)^2 dx$$

$$+ \frac{1}{2} \sum_{i=1}^{2} c_{T,i} \left(\frac{\partial w(x_i)}{\partial x_i} \right)^2 + \frac{1}{2} \int_{-l/2}^{+l/2} \bar{k}_w (w(x))^2 dx + \frac{1}{2} \int_{-l/2}^{+l/2} \bar{k}_s \left(\frac{\partial w(x)}{\partial x} \right)^2 dx, \qquad (2.2)$$

while the work of loads could be described as

$$W = \frac{1}{2} \int_{-l/2}^{+l/2} N \left(\frac{\partial w(x)}{\partial x} \right)^2 dx + \int_{-l/2}^{+l/2} M \frac{\partial^2 w(x)}{\partial x^2} dx, \qquad (2.3)$$

where $w(x)$ is the deflection, E_f is Young's modulus, $I_{y,f}$ is the moment of inertia, G_f is the shear modulus and A_f is the cross section of the fibre. Corresponding to that, the properties of the matrix are represented by the Winkler foundation $\bar{k}_w$ and the Pasternak foundation $\bar{k}_s$. Owing to the uncertainty of the support and its influence on the region, a torsion spring c_T is designated on both sides of the fibre. At the end of the fibre, the axial force N and the bending moment M are applied. For the determination of the deformation of the fibre, a sinusoidal solution is chosen which gives exact results when the Ritz method is used. The deflection $w(x)$ and the angle of the neutral axis $\psi(x)$ perpendicular to the fibre are given by

$$w(x) = \sum_{m=1}^{n} a_m \cos \left(\frac{m\pi x}{l} \right) \quad \text{and} \quad \psi(x) = \sum_{m=1}^{n} b_m \sin \left(\frac{m\pi x}{l} \right), \qquad (2.4)$$

where a_m and b_m represent the amplitude of the deflection and rotation, respectively, and m/l the wavelength of the fibre. The boundary conditions of the model are

$$w \left(-\frac{l}{2} \right) = 0, \quad w \left(+\frac{l}{2} \right) = 0 \quad \text{and} \quad \psi(0) = 0. \qquad (2.5)$$

As a result of the integration and derivation the potential energy Π (equation (2.1)) can be written as

$$\Pi(a_m, b_m) = \frac{1}{4l} m^2 \pi^2 N a_m^2 - \frac{2}{l} m\pi M a_m - \frac{1}{4l} m^2 \pi^2 E_f I_{y,f} b_m^2$$

$$- \frac{1}{4l} \kappa G_f A_f (m\pi a_m - l b_m)^2 \frac{1}{l} m^2 \pi^2 c_T a_m^2 - \frac{1}{4} l \bar{k}_w a_m^2 - \frac{1}{4l} m^2 \pi^2 \bar{k}_s a_m^2, \qquad (2.6)$$

depending on the unknown coefficients a_m and b_m. If it is assumed that the moment M is negligible, the critical buckling load N_{cr} can be derived from the minimum of the potential energy,

$$\frac{\partial \Pi}{\partial a_m} = 0 \quad \text{and} \quad \frac{\partial \Pi}{\partial b_m} = 0, \qquad (2.7)$$

to be

$$N_{cr} = \frac{m^2 N_E}{1 + m^2 N_E / \kappa G_f A_f} + \frac{4}{l} c_T + \frac{l^2}{m^2 \pi^2} \bar{k}_w + \bar{k}_s. \qquad (2.8)$$

In this equation, N_E describes the case of Euler buckling ($N_E = \pi^2/l^2 E_f I_{y,f}$) of a fibre pinned at both ends [17]. In general, it is considered that for $l \to 0$ the equation leads to

$$\lim_{l \to 0} N_{cr} = \kappa G_f A_f \qquad (2.9)$$

and for $l \to \infty$, the critical buckling load becomes

$$\lim_{l \to \infty} N_{cr} = 2 \sqrt{\bar{k}_w E_f I_{y,f}} + \bar{k}_s. \qquad (2.10)$$

Using the definition of Winkler/Pasternak foundation $\bar{k}_w = E_m/l_0 b(d_f)$ and $\bar{k}_s = GA = Gl_0 b(d_f)$, it can be shown that the critical buckling load depends on the thickness of the matrix layer l_0 and the effective width of the fibre foundation $b(d_f)$. According to the size of l_0, the first or the second term of equation (2.10) will vanish, respectively. However, in the case of an eccentricity load,
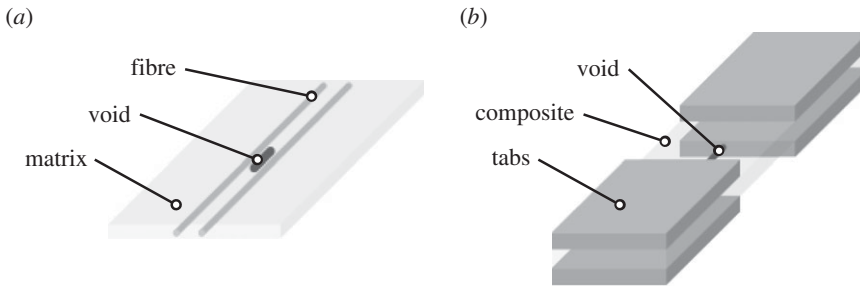
Figure 4. Sketch of model composite specimens consisting of a unique void squeezed between (*a*) two/few fibres or (*b*) two rovings, respectively.

a moment M exists and a non-trivial solution for a_m and b_m out of the potential energy Π can be derived as

$$a_m = \frac{a_0}{N_{cr}/N - 1} \quad \text{and} \quad b_m = \frac{m\pi}{l(1 + m^2 N_E/\kappa G_f A_f)} \frac{a_0}{N_{cr}/N - 1}. \tag{2.11}$$

In this case, a_0 is considered as the initial deflection of the fibre.

(b) Experimental study

(i) Materials and sample preparation

To support the analytical approach a model composite was adapted and manufactured as presented by the authors in [8,9]. It consists of E-glass fibres provided by P-D Glasseiden GmbH (Oschatz, Germany) with a mean diameter of $\bar{d}_f = 70\,\mu\text{m}$ embedded in an epoxy matrix, RIM135 provided by Hexion (Germany). During sample preparation an air bubble was injected into the liquid epoxy using a syringe and squeezing the air bubble between the fibres. This procedure allows one to manufacture specimens consisting of a unique void embedded between two fibres rather than between two rovings. Followed by a curing process at 80°C for 15 h, as recommended by the resin manufacturer, the specimens are removed from the mould, dressed and prepared for testing, as shown in figure 4.

(ii) Compression tests

The compression tests were carried out using a test rig fitting in a transmission light microscope. All specimens were stabilized using an anti-buckling guide. The load was transferred via the end faces (figure 4*a*) of the specimens or end tabs (figure 4*b*), respectively. A cut-out within the anti-buckling guide allowed *in situ* observations using photoelasticity and digital image correlation (DIC; Aramis, provided by GOM mbH). All measured data of force and displacement were recorded continuously with the DigiVision v. 2011.1.0 software provided by Burster.

3. Results

(a) Analytical approach

The critical buckling load N_{cr} of a single fibre in the vicinity of a void could be determined using equations (2.8) and (2.10). In this case, the fibre will lose stability immediately after the critical buckling load is exceeded. There are two states of equilibration:

(i) stable (below critical buckling load) and
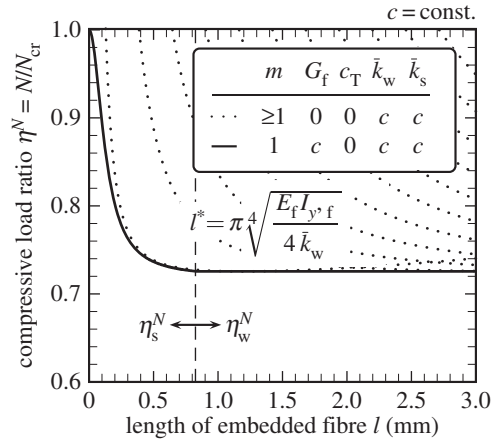(ii) unstable (deflection will become infinite).

6

rsta.royalsocietypublishing.org *Phil. Trans. R. Soc. A* **374**: 20150279

Figure 5. Compressive load ratio η^N as a function of half-embedded fibre length l.
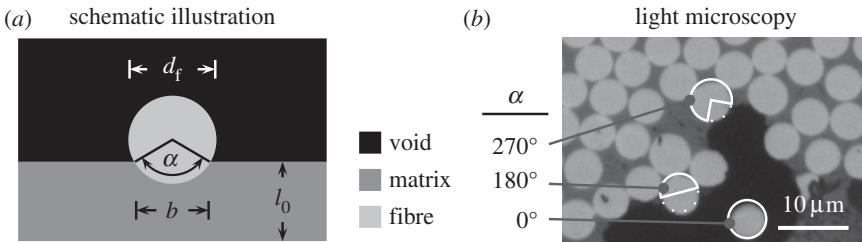

Figure 6. (*a*) Foundation angle α of a fibre dependent on foundation width $b(d_f)$. (*b*) Light micrograph of a CFRP (M21/T800S) cross section in the presence of a void highlighting the scope of the fibre foundation.

Figure 5 shows the compressive load ratio η^N, i.e. compressive load N divided by the critical buckling load N_{cr}, as a function of the length l of a half-embedded fibre. As highlighted in figure 5, the length l^* characterizes the intersection point between the wrapped curves based on equations (2.10) and (3.1):

$$\eta_s^N = \frac{N_E/(1 + N_E/\kappa G_f A_f) + \bar{k}_s}{\kappa G_f A_f + \bar{k}_s} \quad \text{and} \quad \eta_w^N = \frac{2\sqrt{\bar{k}_w E_f I_{y,f}} + \bar{k}_s}{\kappa G_f A_f + \bar{k}_s}. \tag{3.1}$$

For $l < l^*$, the buckling load is dominated by the shear properties of the constituents (fibre and matrix) as well as the flexural property of the fibre. Whereas for $l > l^*$, the stiffness of the matrix E_m, including Winkler foundation $\bar{k}_w$, becomes more significant. It should be mentioned that the compressive load ratio η_w^N is independent of the length of the embedded fibre.

Derived from equation (3.1), it is obvious that the buckling behaviour of the fibre is affected by the Winkler/Pasternak foundation modulus $\bar{k}_w$ and $\bar{k}_s$, respectively. Owing to the two-dimensional view, both parameters are dependent on the effective foundation width b of the matrix. Simplified, the matrix cross section could be reduced to the product of foundation thickness l_0 and foundation width b, as shown in figure 6. In addition, the effective foundation width is based on the foundation angle α. Beside the schematic illustration a light microscopy image of a carbon-fibre-reinforced polymer (CFRP; M21/T800S) cross section in the presence of a void was taken to highlight the scope of the fibre foundation. Unsupported fibres and half- or almost fully embedded fibres are detectable.

The influence of the effective foundation width b or the foundation angle α on the foundation modulus $\bar{k}_w$ and $\bar{k}_s$, respectively, is shown in figure 7. Therefore, equation (3.2), which depends
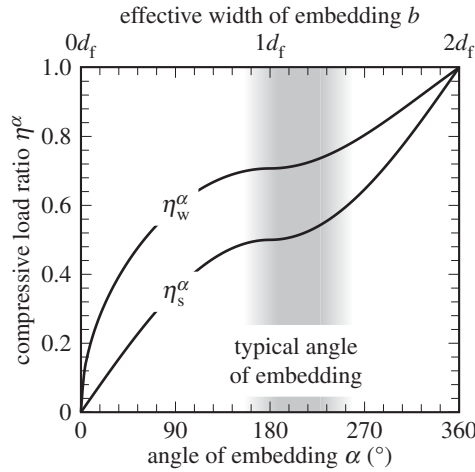
Figure 7. Compressive load ratio η^α as a function of the foundation angle α.

on the effective foundation width, was referred to a full embedded fibre:

$$\eta^\alpha = \frac{2\sqrt{E_m/l_0 b(d_f) E_f I_{y,f}} + G_m l_0 b(d_f)}{2\sqrt{E_m/l_0 2d_f E_f I_{y,f}} + G_m l_0 2d_f}. \tag{3.2}$$

The effective foundation width b could be determined in a simplified view to

$$b(d_f) = \begin{cases} d_f \sin \dfrac{\alpha}{2}, & 0° \leq \alpha < 180°, \\ 2d_f - d_f \sin \dfrac{\alpha}{2}, & 180° \leq \alpha < 360°. \end{cases} \tag{3.3}$$

In particular, the compressive load ratio η^α (equation (3.2)) depends on the variable foundation thickness l_0. For small values of l_0 the compressive load ratio η^α becomes

$$\lim_{l_0 \to 0} \eta^\alpha = \eta_w^\alpha = \sqrt{\frac{b(d_f)}{2d_f}}, \tag{3.4}$$

whereas for large values of foundation thickness l_0, the second term of equation (3.2) dominates,

$$\lim_{l_0 \to \infty} \eta^\alpha = \eta_s^\alpha = \frac{b(d_f)}{2d_f}. \tag{3.5}$$

Equations (3.4) and (3.5) form limiting curves, as shown in figure 7. In general, the compressive load ratio η^α increases with increasing foundation thickness from the basis η_w^α to η_s^α. In the case of half-embedded fibres, the influence of the foundation thickness is clearly visible. However, the critical compressive load ratio η_w^α reaches 70%, whereas the compressive load ratio η_s^α is only 50% of the maximum load.

The comparison between the effective foundation and the influence of fibre orientation is a subject of special interest. Using the assumption of elliptical cross sections of voids, the foundation angle of single fibres is conducted to $\alpha > 180°$, so that the compressive load ratio could be fixed to 0.5 and 0.7, respectively.

In the previous section, it was assumed that the applied moment is negligible. In that case the fibre changes the state of equilibration immediately from stable to unstable. However, owing to void inclusions, the load introduction is hardly perfect, so it is necessary to identify the influence of an applied moment. For example, voids could cause a fibre misalignment leading to a distorted or an eccentric load introduction, respectively. The applied load N induces a bending moment M, which leads to a further distortion of the fibre a_m. Figure 8 shows the compressive load ratio η^ϕ
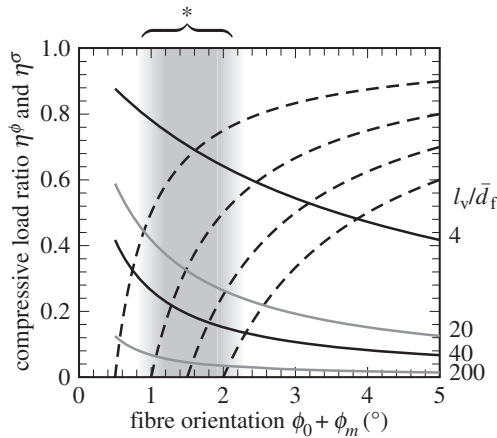
Figure 8. Compressive load ratio η^ϕ and η^σ as a function of relative fibre orientation $\phi_0 + \phi_m$ and fibre diameter (glass fibre $\bar{d}_{f,G} = 25\,\mu$m and carbon fibre $\bar{d}_{f,C} = 5\,\mu$m). Asterisk denotes typical range of ϕ_0, see also table 1.

based on equation (2.11) as a function of the relative fibre orientation $\phi_0 + \phi_m$. With increasing compressive load ratio η^ϕ, the relative deflection also increases. For all cases shown in figure 8 (dashed lines), the compressive load ratio converges asymptotically to the critical buckling load of the perfectly aligned fibre. To determine the point at which the curves become physically relevant, it is necessary to draw down curves of stress [18]. Owing to its distortion the compressive stress ratio η^σ could be calculated by the superposition principle between compressive and bending loads. Based on linear elastic material behaviour, the compressive load ratio η^σ can be determined from fibre failure in compression and the applied stress, respectively [18–20]. Then, the compressive load ratio η^σ (equation (3.6)) can be simply written as

$$\eta^\sigma = \frac{1}{1 + 8(a_0/l + a_m/l)(l_v/\bar{d}_f)}, \tag{3.6}$$

where $a_0/l + a_m/l$ can be transferred to fibre orientation angle $\phi_0 + \phi_m$. Two typical $l_v/\bar{d}_f$ ratios (glass fibre $\bar{d}_{f,G} = 25\,\mu$m and carbon fibre $\bar{d}_{f,C} = 5\,\mu$m depending on length of void $l_v = 0.1$ mm and $l_v = 1.0$ mm, respectively [21]) are plotted as hyperbolae (solid lines) in figure 8. This approach of Mies [18] and Hahn [20] is concluded as acceptable, to determine the compressive strength of a $0°$ unidirectional laminate by Berbinau *et al.* [22]. However, in this case figure 8 clearly illustrates that the fibre diameter has a significant influence on failure behaviour under compressive load, which was neglected by the approach of Argon [23] and Budiansky [7].

(b) Experimental study

The experimental study on micro- and meso-scales allows the investigation of the stress conditions, failure initiation and the failure propagation due to void inclusions. Therefore, a photoelastic as well as a DIC study of the model composites as a function of several aspect ratios of the void (length/width: l_v/b_v) were performed, as shown in figures 9 and 10, respectively. In this case, it should be mentioned that the photoelasticity was used to visualize the stability behaviour of the fibre. The dashed lines represent the stress-induced buckling of the fibres. It could be observed that along the void inclusion different fringe patterns occur. Especially for a void aspect ratio >1 typical shapes of stress concentrations appear (blue colour online) around the void and along its closest fibre, which offers valuable hints to the buckling of the fibres. Similar results concerning the photoelastic pattern of fibres under compression were observed by Rosen [10], who investigated the compressive behaviour of composites on fully embedded fibres. It can be concluded that the reduced support of fibres leads to buckling of fibres near the voids.
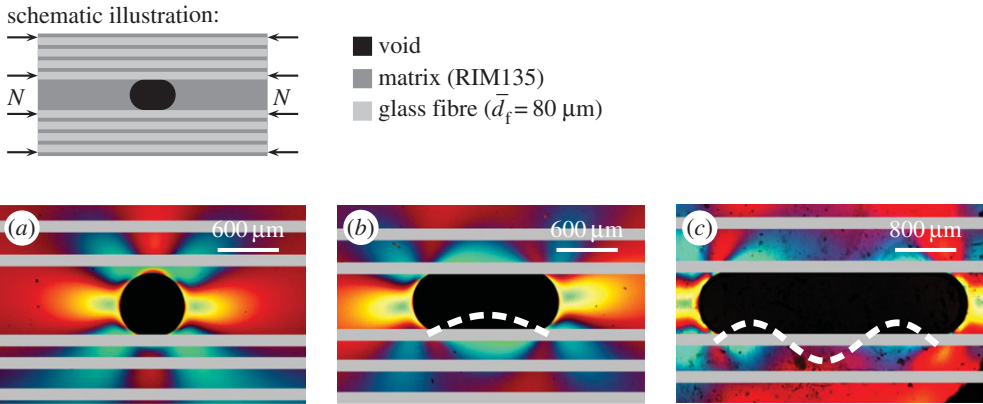
Figure 9. Photoelastic study (white light) of model composite (eight fibres) depending on aspect ratio of the void. (a) $l_v/b_v = 1$ ($N = 260$ N); (b) $l_v/b_v = 2.3$ ($N = 250$ N) and (c) $l_v/b_v = 3.8$ ($N = 276$ N) [8].
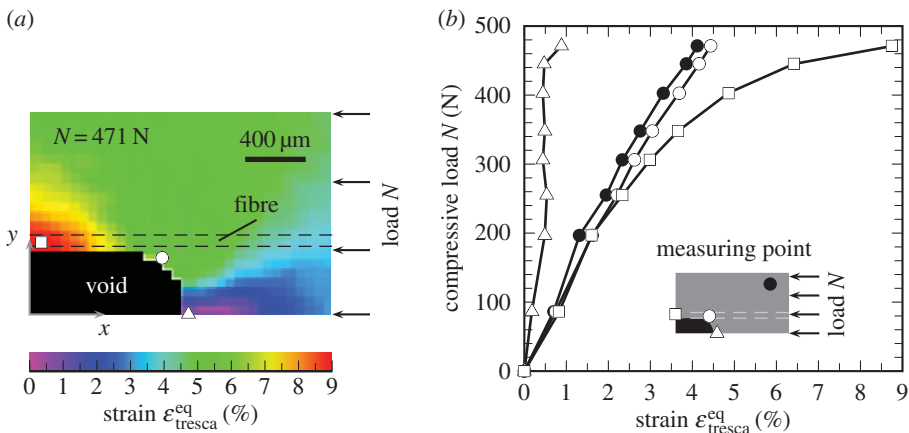

Figure 10. Contour plot (DIC measurement) of strain in the vicinity of a unique void (a) and selected measuring points of strain dependent on the compressive load (b).

Further experimental studies on model composites (micro-scale) were performed using DIC evaluation (Figure 10) shows a contour plot of the equivalent strain $\varepsilon_{\text{tresca}}^{\text{eq}}$ on the surface of the model composite (figure 10a) and a diagram of selected measuring points of interest (figure 10b). The minimum and maximum strain are located in the summit ($\varepsilon_{\text{tresca}}^{\text{eq,min}} = 0.2\%$) and in the middle ($\varepsilon_{\text{tresca}}^{\text{eq,max}} = 8.7\%$) of the void, respectively. In contrast with observations based on photoelasticity, shear stresses (circles) induced by stress rearrangements at the end cap of the void are negligible. Thus, the maximum strain is dominated alongside the void from fibres deflected into the void initiating fibre kinking (squares). At this point, the matrix deforms already nonlinearly, even at low compressive load ($N = 325$ N or rather $\sigma^c = 40$ MPa).

The failure initiation and propagation could also be conducted on meso-scale (model composites manufactured using rovings instead of a few fibres). Figure 11a shows the cross section of a model composite in which a kink-band has been formed. As pointed out in figure 9c, the fibre kinking took place alongside the void at a point of high stress concentration. It seems that first a damage zone is formed, as shown in figure 11b in the background, followed by kinking of fibres near the void into the free volume [8,24].
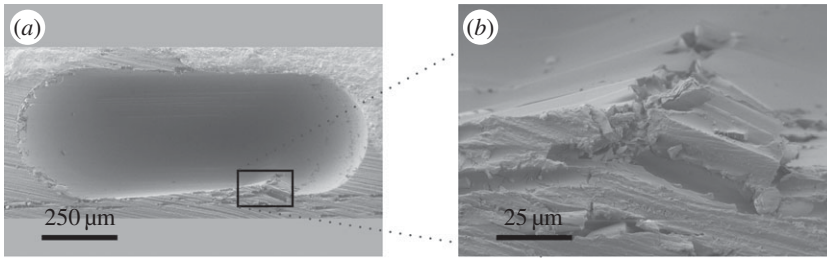
Figure 11. (*a*) SEM picture of a cross section of a model composite showing a kink-band and (*b*) high magnification of kink-band.

4. Discussion

(a) Representativeness of the model

The assumptions based on CFRP laminates may be too simple to represent real composites containing voids. However, the derived model (figure 2) could also be found at a cutaway view of CFRP, published in a separate paper [8]. Particularly, for third-generation prepreg systems the formation of voids partly takes place within resin-rich areas [25]. Thus, the absolutely reduced model (focusing on area III, figure 3) is also reasonable. In this case, one has to think about the assumption seriously that fibres are adapted to void geometry as a sinusoidal curve, as shown in other publications [4,26]. Owing to the fact that interlaminar voids hardly affect the fibre orientation, an estimation of the compressive strength based on fibre orientation alone would be inappropriate.

In general, the specimens were manufactured by using glass fibres and rovings, respectively. This allows the investigation of stress–strain conditions in the matrix around a unique void by using optical evaluation methods such as light transmission microscopy, photoelasticity and DIC. These investigations also show that the analytical approach should be extended by implementing nonlinear material behaviour of the matrix if the compressive strength could be predicted.

(b) Compressive failure in the presence of voids

Assuming there are two types of voids (intralaminar and interlaminar) most of them occur between plies in resin-rich areas [21,27,28]. However, it is obvious to apply an established theory, like Budiansky's approach [7], to predict the compressive strength indirectly for composites containing voids, as suggested by Lee & Soutis [6]. Therefore, the initial fibre orientation has to combine with the void content. Assuming a Gaussian distribution, the standard deviation of fibre orientation is determined based on studies on M21/T800S by using Yurgartis' method [29,30]. This is summarized in table 1. Taking into account an initial fibre orientation of $\phi_0 = 1° – 2°$, this practice would lead to a reduction of the compressive strength of less than 30%, depending on fibre diameter (cf. figure 8). Given that the fibre diameter is not considered in Budiansky's theory, the resistance of thick fibres against microbuckling could not be taken into account anyway [2]. In addition, with increasing fibre alignment the compressive load ratio will decrease asymptotically to a negligible value. Hence, the compressive load ratio would be underestimated.

In general, just a couple of publications could be found with experimental data[1] about compressive strength as a function of void contents between $v_v = 0\%$ and $\approx 25\%$, as summarized in figure 12. In combination with findings of failure initiation, as shown in figure 11 and presented in [8], equation (3.2) leads to a minimum in compressive strength $\eta \approx 50\%$ for half-embedded fibres. As observed in experimental studies for model composites at the micro- and meso-scale levels, the failure initiation is caused by fibre–matrix debonding [32–34], which could be pushed

---

[1]Owing to the fact that fibres were soaked in acetone before being saturated with resin to increase void contents, experimental data of Hancox [31] are not considered.
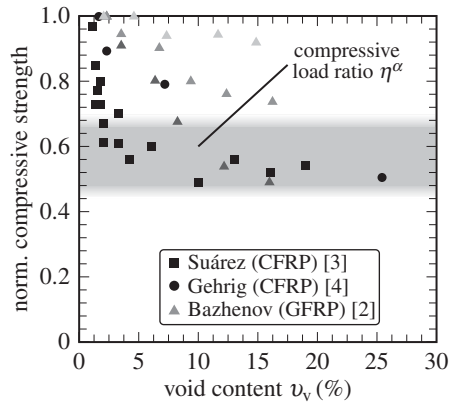
Figure 12. Normalized compressive strength of different composite laminates depending on void content [2–4]. Measurement data: Gehrig (CFRP) are mean values, whereas Bazhenov (GFRP) also investigated the influence of fibre diameter: $\bar{d}_f = 19\,\mu m$ (black triangle), 80 μm (dark grey triangle) and 130 μm (light grey triangle).

Table 1. Standard deviation of fibre misalignment in plane ϕ_0^{ip} and out of plane ϕ_0^{op} depending on void content v_v. Measurement data of fibre misalignment are based on studies on M21/T800S by using Yurgartis' method [29,30].

void content, v_v (%)	≤0.1	2.7	6.8	9.0
autoclave pressure (bar)	7	5	3	1
fibre misalignment, ϕ_0^{ip} (°)	0.9	1.1	0.8	1.3
fibre misalignment, ϕ_0^{op} (°)	1.3	1.4	1.5	2.8

by fibre misalignment, followed by kink-band formation [8,26]. This leads to the assumption that the foundation (fibre–matrix bond) dominates the failure process.

(c) Transfer from model to real composite

The role of the matrix while loading is most important as it supports and controls the microbuckling behaviour of the embedded fibres, as shown in figures 9 and 10. In contrast with numerical studies in which just idealized models could be analysed, the simplicity of this approach allows one to investigate failure modes on model composites and to transfer the results to real composites. As shown in figure 11, failure initiation occurs in overloaded areas of the matrix (figures 9 and 10). Furthermore, the failure modes of composites [8] are in accordance with failure mechanisms on model composite [8].

Owing to the fact that the basic principles of the analytical approach are independent of mechanical properties for different materials (figures 7 and 8), the findings from this study should also be transferable to all fibre-reinforced materials.

5. Conclusion

For this work, a hierarchical approach was chosen to investigate the degradation process in composites containing void inclusions under compressive load. By using an analytical approach it could be shown that the mechanical behaviour of fibre-reinforced composites is significantly influenced by the stiffness of both matrix and fibre and the fibre–matrix bonding, further by the initial fibre orientation and the fibre diameter. Voids lead to local stress concentrations in the matrix which are enhanced by fibre distortion into the void volume. There are generally two different limiting factors influencing the compressive strength of composites in the presence of

voids. First, the fibre orientation leading to premature microbuckling, particularly in the case of a low void content. Second, the embracement of fibres with matrix (angle of fibre embedded in the matrix) which can result in a 50% maximum loss of compressive strength. This is evident also from experimental data of several publications.

Finally, in the authors' opinion, the determination of the compressive strength of composites in the presence of voids should consider not just the void content but more importantly the critical number of affected fibres using a probabilistic approach. Owing to the fact that the formation of voids cannot be avoided during the manufacturing process of composites, the presented approach has to be extended to further load cases, e.g. transverse tensile, shear loading. This would create the possibility to integrate a parameter of failure criteria to estimate the upper and lower bounds for critical loads in the phase of design. The precondition, therefore, is whether a critical size/position or certain amount of voids exists and how voids influence the mechanical behaviour under various load cases.

References

1. Port KF. 1982 The compressive strength of carbon fiber reinforced plastics. Technical report no. 82083. Royal Aircraft Establishment, Farnborough, UK.
2. Bazhenov SL, Kuperman AM, Zelenskii ES, Berlin AA. 1992 Compression failure of unidirectional glass-fibre-reinforced plastics. *Compos. Sci. Technol.* **45**, 201–208. (doi:10.1016/0266-3538(92)90080-M)
3. Suárez JC, Molleda F, Güemes A. 1993 Void content in carbon fibre/epoxy resin composites and its effects on compressive properties. In *Proc. 9th Int. Conf. on Composite Materials (ICCM-9), Madrid, Spain, 12–16 July*, vol. VI, *Composites properties and applications* (ed. A Miravete), pp. 589–596. University of Zaragoza; and Cambridge, UK: Woodhead.
4. Gehrig F. 2011 The influence of pores on the damage behaviour of carbon fibre-reinforced polymers. Ph.D. thesis, Technische Universität Hamburg-Harburg, Germany. [In German].
5. Schultheisz CR, Waas AM. 1996 Compressive failure of composites. *Prog. Aerosp. Sci.* **32**, 1–78. (doi:10.1016/0376-0421(94)00002-3)
6. Lee J, Soutis C. 2007 A study on the compressive strength of thick carbon fibre–epoxy laminates. *Compos. Sci. Technol.* **67**, 2015–2026. (doi:10.1016/j.compscitech.2006.12.001)
7. Budiansky B. 1983 Micromechanics. *Comput. Struct.* **16**, 3–12. (doi:10.1016/0045-7949(83)90141-4)
8. Liebig WV, Viets C, Schulte K, Fiedler B. 2015 Influence of voids on the compressive failure behaviour of fibre-reinforced composites. *Compos. Sci. Technol.* **117**, 225–233. (doi:10.1016/j.compscitech.2015.06.020)
9. Liebig WV, Leopold C, Schulte K. 2013 Photoelastic study of stresses in the vicinity of a unique void in a fibre-reinforced model composite under compression. *Compos. Sci. Technol.* **84**, 72–77. (doi:10.1016/j.compscitech.2013.04.011)
10. Rosen BW. 1965 Mechanics of composite strengthening. In *ASM Seminar on Fiber Composite Materials, Philadelphia, PA, 17–18 October 1964*, pp. 37–75. Metals Park, OH: American Society for Metals.
11. Gutkin R, Pinho ST, Robinson P, Curtis PT. 2010 On the transition from shear-driven fibre compressive failure to fibre kinking in notched CFRP laminates under longitudinal compression. *Compos. Sci. Technol.* **70**, 1223–1231. (doi:10.1016/j.compscitech.2010.03.010)
12. Wisnom MR. 1990 The effect of fibre misalignment on the compressive strength of unidirectional carbon fibre/epoxy. *Composites* **21**, 403–407. (doi:10.1016/0010-4361(90)90438-3)

13. Engesser F. 1891 Die Knickfestigkeit gerader Stäbe. *Zentralbl. Bauverwaltung* **11**, 483–486.
14. Timoshenko SP, Gere JM. 1961 *Theory of elastic stability*, 2nd edn. New York, NY: McGraw-Hill.
15. Winkler E. 1867 *Die Lehre von der Elasticitaet und Festigkeit mit besonderer Rücksicht auf ihre Anwendung in der Technik*. Prague, Czech Republic: Dominicus.
16. Pasternak PL. 1954 On a new method of analysis of an elastic foundation by means of two foundation constants. In *Gosudarstvennoe Izdatelstvo Literaturi po Stroitelstvu i Arkhitekture*. [In Russian.]
17. Euler L. 1744 *Methodus Inveniendi Lineas Curvas Maximi Minimive Proprietate Gaudentes, Sive Solutio Problematis Isoperimetrici Latissimo Sensu Accepti*. Lausanne, Switzerland: Marcum Michaelem Bousquet.
18. Mies O. 1912 Über das Ausknicken stabförmiger Körper. *Dinglers Polytechnisches J.* **327**, 177–181.
19. Ostenfeld A. 1898 Exzentrische und zentrische Knickfestigkeit. *VDI-Z* **94**, 1462–1470.
20. Hahn HT. 1987 Analysis of kink band formation under compression. In *Proc. 6th Int. Conf. on Composite Materials and 2nd European Conf. on Composite Materials (ICCM-6/ECCM-2), London, UK, 20–24 July* (ed. FL Matthews *et al.*), vol. 1, pp. 269–277. London, UK: Elsevier Applied Science.
21. Huang H, Talreja R. 2005 Effects of void geometry on elastic properties of unidirectional fiber reinforced composites. *Compos. Sci. Technol.* **65**, 1964–1981. (doi:10.1016/j.compscitech.2005.02.019)
22. Berbinau P, Soutis C, Guz IA. 1999 Compressive failure of $0°$ unidirectional carbon-fibre-reinforced plastic (CFRP) laminates by fibre microbuckling. *Compos. Sci. Technol.* **59**, 1451–1455. (doi:10.1016/S0266-3538(98)00181-X)
23. Argon AS. 1972 Fracture of composites. *Treatise Mater. Sci. Technol.* **1**, 79–114. (doi:10.1016/B978-0-12-341801-2.50007-2)
24. Garland BD, Beyerlein IJ, Schadler LS. 2001 The development of compression damage zones in fibrous composites. *Compos. Sci. Technol.* **61**, 2461–2480. (doi:10.1016/S0266-3538(01)00176-2)
25. Liebig WV, Gehrig F, Schulte K. 2010 Influence of voids on the behaviour of composites. In *Proc. 14th Eur. Conf. on Composite Materials, Budapest, Hungary, 7–10 June* (eds L Kollár, T Czigány, J Karger-Kocsis). Budapest University of Technology and Economics, Department of Polymer Engineering.
26. Hapke J, Gehrig F, Huber N, Schulte K, Lilleodden ET. 2011 Compressive failure of UD-CFRP containing void defects: in situ SEM microanalysis. *Compos. Sci. Technol.* **71**, 1242–1249. (doi:10.1016/j.compscitech.2011.04.009)
27. Olivier P, Cottu JP, Ferret B. 1995 Effects of cure cycle pressure and voids on some mechanical properties of carbon/epoxy laminates. *Composites* **26**, 509–515. (doi:10.1016/0010-4361(95)96808-J)
28. Howe CA, Paton RJ, Goodwin AA. 1997 A comparison between voids in RTM and prepreg carbon/epoxy laminates. In *Proc. 11th Int. Conf. on Composite Materials, Gold Coast, Queensland, Australia, 14–18 July* (ed. ML Scott), vol. IV, *Composites processing and microstructure*, pp. 46–51. Melbourne, Australia: Australian Composite Structures Society. See http://www.iccm-central.org/Proceedings/ICCM11proceedings/ICCM_11v4.pdf.
29. Yurgartis SW. 1987 Measurement of small angle fiber misalignments in continuous fiber composites. *Compos. Sci. Technol.* **30**, 279–293. (doi:10.1016/0266-3538(87)90016-9)
30. Liebig W. 2014 A micromechanical approach to investigate the influence of voids on properties of fibre-reinforced polymers. Ph.D. thesis, Technische Universität Hamburg-Harburg, Germany. [In German].
31. Hancox NL. 1975 The compression strength of unidirectional carbon fibre reinforced plastic. *J. Mater. Sci.* **10**, 234–242. (doi:10.1007/BF00540347)
32. Guz IA, Soutis C. 2000 Critical strains in layered composites with interfacial defects loaded in uniaxial or biaxial compression. *Plastic Rubber Compos.* **29**, 489–495. (doi:10.1179/146580100101541346)
33. Guz IA, Soutis C. 2001 Predicting fracture of layered composites caused by internal instability. *Composites A* **32**, 1243–1253. (doi:10.1016/S1359-835X(01)00077-X)
34. Soutis C, Guz IA. 2006 Fracture of layered composites by internal fibre instability: effect of interlaminar adhesion. *Aeronaut. J.* **110**, 185–195. (doi:10.1017/S0001924000001160)